Analysis of Crack Propagation in Fixed-Free Single-Walled Carbon Nanotube Under Tensile Loading Using XFEM

Anand Y. Joshi
e-mail: anandyjoshi@gmail.com

Satish C. Sharma
e-mail: sshmefme@iitr.ernet.in

S. P. Harsha
e-mail: surajfme@iitr.ernet.in

Department of Mechanical and Industrial Engineering,
Vibration and Noise Control Laboratory,
Indian Institute of Technology, Roorkee,
Roorkee 247667,
Uttarakhand, India

Fracture mechanics at the nanoscale level is a very complex phenomenon, whereas the macroscale fracture mechanics approach can be employed for nanoscale to simulate the effect of fracture in single-walled carbon nanotubes (SWCNTs). In this study, an extended finite element method is used to simulate crack propagation in carbon nanotubes. The concept of the model is based on the assumption that carbon nanotubes, when loaded, behave like space frame structures. The nanostructure is analyzed using the finite element method, and the modified Morse interatomic potential is used to simulate the nonlinear force field of the C–C bonds. The model has been applied to single-walled zigzag, armchair, and chiral nanotubes subjected to axial tension. The contour integral method is used for the calculation of the J-integral and stress intensity factors (SIFs) at various crack locations and dimensions of nanotubes under tensile loading. A comparative study of results shows the behavior of cracks in carbon nanotubes. It is observed that for the smaller length of nanotube, as the diameter increased, the stress intensity factor is linearly varied while for the longer nanotube, the variation in stress intensity factor is nonlinear. It is also observed that as the crack is oriented closer to the loading end, the stress intensity factor shows higher sensitivity to smaller lengths, which indicates more chances for crack propagation and carbon nanotube breakage. The SIF is found to vary nonlinearly with the diameter of the SWCNT. Also, it is found that the predicted crack evolution, failure stresses, and failure strains of the nanotubes correlate very well with molecular mechanics simulations from literature. [DOI: 10.1115/1.4002417]

Keywords: XFEM, carbon nanotubes, contour integral method

1 Introduction

Carbon nanotubes (CNTs) with their unique structures have been the most interesting nanostructures ever introduced due to their exceptionally superior mechanical, thermal, electrical, and optical properties. The properties of CNTs have strong dependency on their structural configurations (i.e., armchair, zigzag, and chiral), the number of their concentric inner shells (i.e., single-walled, double-walled, and multiwalled), and their structural defects and impurities. The hybrid molecular nanoscale structures with their tunable functionality are excellent candidates in a wide range of applications, which have been investigated and examined [1–3].

CNTs have superior properties compared with traditional engineering materials. However, these properties hold only for the ideal case of carbon nanotubes, where these are made of perfect hexagonal graphite honeycomb lattice of mono-atomic layer thickness. The advantages or disadvantages of the presence of defects in carbon nanotubes depend on their applications. Structural defects may increase the adhesion of other atoms and molecules to carbon nanotubes. The possibility of connecting two nanotubes with different chiralities by introducing heptagon and pentagon in the perfect hexagonal graphite lattice was addressed by Dunlap [4]. Recently, it has been shown that a wavy CNT with and without attached mass shows periodic and different nonlinear behaviors as mass is attached at different positions along the length [5]. Also, the effect of pinhole defects and the atomic vacancies on the dynamic behavior of single-walled carbon nanotube (SWCNT) based mass sensors have been examined [6,7]. Further, it has been reported that SWCNT based mass sensors exhibit superharmonic and subharmonic responses with different levels of mass [8]. It has been observed [9] that with the increase in the attached mass on the CNT, the vibration spectra of CNT show a dense signature near the peak of excitation, which appears to have a chaotic nature with reduced vibration amplitude.

Experimental observations have revealed that topological defects, such as the Stone–Wales defect and vacancy defects, are commonly present in CNTs [10]. Defects degrade the mechanical performance of CNTs since they alter not only their inelastic properties but also the elastic properties such as the Young's modulus and Poisson's ratio. The longitudinal and transverse stiffnesses as well as the flexural rigidity in tension, torsion, and bending are, consequently, being altered. For example, Chandra et al. [11] showed that the presence of the Stone–Wales defect reduces the stiffness of the defected area by about 30–50%, resulting in the reduction of the nanotube Young's modulus.

The studies that considered such effect and, therefore, gave information about the mechanical performance of CNTs were the simulations of Belytschko et al. [12], Mielke et al. [13], and Liew et al. [14] as well as the measures of stress and strain at the atomic scale of Chandra et al. [11]. Belytschko et al. [12] studied the fracture of CNTs under axial tension by molecular mechanics (MM) simulations. They found that the fracture behavior is almost independent of the separation energy and dependent on the inflection point of the interatomic potential. The failure strain of a zigzag nanotube was predicted to be between 10% and 15%, which compares reasonably well with the experimental results. Contrary to failure strain, the failure stresses were found to be 65–93 GPa, which are markedly higher than the experimental ones.

Manuscript received June 11, 2010; final manuscript received August 18, 2010; published online October 22, 2010. Editor: Vijay K. Varadan.

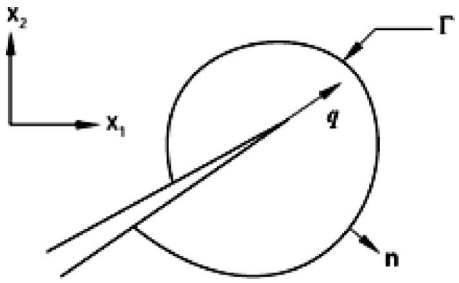

Fig. 1 J-integral in two dimensions

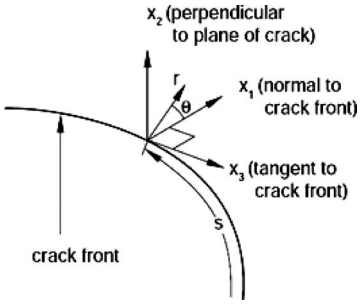

Fig. 2 J-integral in three dimensions

In this paper, a solid modeling technique is used for simulating the crack propagation phenomena in CNT using the extended finite element method (XFEM) and other various fracture parameters, such as stress intensity factor (SIF) K_I and J-integral, are calculated using the contour integral method. This paper consists of comparative study of various types of CNT configurations for different crack positions.

2 Fracture Mechanics

Experimental observations and theoretical elasticity helped to create the fundamental aspects of the theory of fracture mechanics. Major differences between the theoretical prediction of tensile strength and the experimentally measured one are the assumption of existing minute flaws and defects, predicting drastic changes in the distribution of the stress field around each flaw regardless of its actual size. The fundamental concepts of stress intensity factor, energy release rate, etc., are used to analyze a crack problem. Energy based methods allow classical fracture mechanics to be extended to nonlinear problems.

J-integral is a powerful numerical tool (similar to the finite element method) to be used for efficiently determining the necessary fields and variables [15].

2.1 J-Integral. The J-integral is widely accepted as a fracture mechanics parameter for both linear and nonlinear material responses. It is related to the energy release associated with crack growth and is a measure of the intensity of deformation at a notch or crack tip, especially for nonlinear materials. If the material response is linear, it can be related to the stress intensity factors. Because of the importance of the J-integral in the assessment of flaws, its accurate numerical evaluation is vital to the practical application of fracture mechanics in design calculations. In the context of quasi-static analysis, the J-integral is given as

$$J = \lim_{\Gamma \to 0} \int_{\Gamma} n \cdot H \cdot q \cdot d\Gamma \tag{1}$$

As shown in Fig. 1, Γ is a contour beginning on the bottom crack surface and ending on the top surface, q is a unit vector in the virtual crack extension direction, and n is the outward normal to Γ. H is given by

$$H = WI - \sigma \cdot \frac{\partial u}{\partial x} \tag{2}$$

For an elastic material behavior, W is the elastic strain energy, and for an elastic-plastic or elastic-viscoplastic material behavior, W is defined as the elastic strain energy density plus the plastic dissipation, thus representing the strain energy in an "equivalent elastic material." The J-integral can be extended to three dimensions (as shown in Fig. 2) by considering a crack with a tangentially continuous front. The local direction of virtual crack extension is, again, given by q, which is perpendicular to the local crack front and lies in the crack plane. Asymptotically, as $r \to 0$, the conditions for path independence apply on any contour in the $x_1 - x_2$ plane, which is perpendicular to the crack front at s. Hence, the J-integral defined in this plane can be extended to represent the pointwise energy release rate along the crack front as

$$J(s) = \lim_{\Gamma \to 0} \int_{\Gamma} n \cdot H \cdot q \cdot d\Gamma \tag{3}$$

For a virtual crack advance in the plane of a three-dimensional crack, the energy release rate is given by

$$\bar{J} = \int_{L} J(s)\lambda(s)ds, \quad \bar{J} = \lim_{\Gamma \to 0} \int_{A_t} \lambda(s) \cdot n \cdot H \cdot q \cdot dA \tag{4}$$

2.2 SIF. The stress intensity factors K_I, K_{II}, and K_{III} play an important role in linear elastic fracture mechanics. They characterize the influence of load or deformation on the magnitude of the crack-tip stress and strain fields and measure the propensity for crack propagation or the crack driving forces. Furthermore, the stress intensity can be related to the energy release rate (the J-integral) for a linear elastic material through

$$J = \frac{1}{8\pi} K^T \cdot B^{-1} \cdot K \tag{5}$$

where $\mathbf{K} = [K_I, K_{II}, K_{III}]^T$ and $\mathbf{B}$ is called the prelogarithmic energy factor matrix [16,17]. For homogeneous, isotropic materials, it is diagonal and the above equation simplifies to

$$J = \frac{1}{\bar{E}}(K_I^2 + K_{II}^2) + \frac{1}{2G} K_{III}^2 \tag{6}$$

where $\bar{E} = E$ for plane stress and $\bar{E} = E/(1-\nu^2)$ for plane strain, axisymmetry, and three dimensions.

For an interfacial crack between two dissimilar isotropic materials with Young's moduli E_1 and E_2, Poisson's ratio ν_1 and ν_2, and shear moduli $G_1 = E_1/2(1+\nu_1)$ and $G_2 = E_2/2(1+\nu_2)$,

$$J = \frac{1-\beta^2}{E^*}(K_I^2 + K_{II}^2) + \frac{1}{2G^*} K_{III}^2 \tag{7}$$

where

$$\frac{1}{E^*} = \frac{1}{2}\left(\frac{1}{E_1} + \frac{1}{E_2}\right), \quad \frac{1}{G^*} = \frac{1}{2}\left(\frac{1}{G_1} + \frac{1}{G_2}\right),$$

$$\beta = \frac{G_1(k_2 - 1) - G_2(k_1 - 1)}{G_1(k_2 - 1) + G_2(k_1 - 1)}$$

where $k = (3-4\nu)$ for plane strain and $k = (3-\nu)/(1+\nu)$ for plane stress.

3 XFEM

Traditional finite element methods are difficult to implement in a crack propagation problem due to the problem of remeshing it as the crack progresses. Moreover, the approximation of the crack-tip singularity should be accurate. XFEM is a numerical method to model internal (or external) boundaries, such as holes, inclusions,

or cracks, without requiring the mesh to conform to these boundaries. It is based on a standard Galerkin procedure and uses the concept of partition of unity [18,19] to accommodate the internal boundaries in the discrete model. XFEM presents a method for enriching finite element approximations so that crack growth problems can be solved with minimal remeshing [20–22]. Later, an enrichment technique that includes the asymptotic near tip field and a Heaviside function $H(x)$ can be used for the three-dimensional static crack modeling [23].

3.1 Crack-Tip Enrichment. Extended finite element method and generalized finite element method [24–27] belong to the class of partition of unity methods and add discontinuous enrichment functions to the finite element approximation using the partition of unity,

$$u(x) = \sum_{i=1}^{n} N_i(x) \left[u_i + \sum_{j=1}^{ne(i)} a_{ji} F_j(r,\theta) \right] \tag{8}$$

where (r,θ) is a polar coordinate system with an origin at the crack tip and $N_i(x)$ are the standard finite element shape functions. The enrichment coefficient a_{ji} is associated with nodes, and $ne(i)$ is the number of coefficients for node I.

The crack-tip enrichment functions in isotropic elasticity $F_i(r,\theta)$ are obtained from the asymptotic displacement fields,

$$\{F_j(r,\theta)\}_{j-1}^{4} = \left\{ \begin{array}{c} \sqrt{r}\sin\left(\frac{\theta}{2}\right) \\ \sqrt{r}\cos\left(\frac{\theta}{2}\right) \\ \sqrt{r}\sin\left(\frac{\theta}{2}\right)\sin(\theta) \\ \sqrt{r}\cos\left(\frac{\theta}{2}\right)\sin(\theta) \end{array} \right\} \tag{9}$$

3.2 Heaviside Function. The Heaviside jump function is a discontinuous function across the crack surface and is constant on each side of the crack +1 on one side and −1 on the other. After intruding this jump function, the approximation will be changed to the following:

$$U = \sum_{i\in 1} u_i N_i + \sum_{j\in J} b_j N_j H(x) + \sum_{k\in K1} N_k \left[\sum_{I=1}^{4} C_k^{i1} F_i^1(x) \right] + \sum_{k\in K2} N_k \left[\sum_{I=1}^{4} C_k^{i2} F_i^2(x) \right] \tag{10}$$

where N_i is the shape function associated to node i, I is the set of all nodes of the domain, J is the set of nodes whose shape function support is cut by a crack, K is the set of nodes whose shape function support contains the crack front, u_i is the classical degree of freedom (i.e., displacement) for node i, and b_j accounts for the jump in the displacement field across the crack at node j. If the crack is aligned with the mesh, b_j represents the opening of the crack, $H(x)$ is the Heaviside function, C_k^1 is the additional degree of freedom associated with the crack-tip enrichment functions, and F_l is an enrichment, which corresponds to the four asymptotic functions in the development expansion of the crack-tip displacement field in a linear elastic solid.

3.3 LSM. The level set method (LSM) is a numerical scheme [28] to model the motion of interfaces. The principle of the method is to represent an interface by the zero of a function called the level set function. A significant advance of the XFEM method is given by its coupling with LSMs. The LSM is used to represent the crack location, including the location of crack tips. The XFEM is used to compute the stress and displacement fields necessary for determining the rate of crack growth.

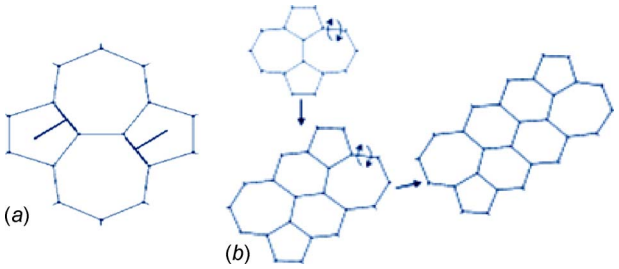

Fig. 3 (*a*) Stone–Wales defect can be seen as a pair of dislocations, where each 5–7 pair represents a dislocation and (*b*) 5–7 pairs are gliding away from each other due to bond reconstructions [29]

4 Glide Dislocations in Carbon Nanotubes

It has been shown [29] that the glide of the dislocations existing in the carbon nanotubes leads to the formation of defects, such as Stone–Wales and vacancies, which further lead to the fracture propagation. The glide of dislocations can be differentiated into two categories.

4.1 Glide of Dislocation by Bond Rotation. By studying the energetics of a pair of edge dislocations in a CNT under axial loading using both MM and XFEM, it is found that the edge dislocation pair is generated by creating a Stone–Wales defect, as shown in Fig. 3(*a*). Ding et al. [30] suggested a glide mechanism in CNTs; the side bond of one of the heptagons of the Stone–Wales defect was rotated by 90 deg, and the bonds were reconstructed so that two separated 5–7 defect pairs were generated, as shown in Fig. 3(*b*). As this process repeats, the tube diameter shrinks as the length increases.

4.2 Climb of Dislocation by Atom Removal. Considering the climb of dislocation pairs due to the removal of atom pairs from the CNT lattice, it was proposed by Ding et al. [30] that the loss of mass observed during experiments performed on CNTs was mainly due to the removal of atom pairs, which leads to the climb motion of a prismatic dislocation [31]. As shown in Fig. 4, a two-atom vacancy can be viewed as a dislocation pair. The removal of pairs of atoms followed by the reconstruction of bonds induces the separation of the dislocation dipole.

Moreover, Ding et al. [30] showed that the results using XFEM matched the molecular mechanics calculations quite well; the energy increased at all the strains with dislocation climb. Thus, XFEM model calculations agree closely with MM models in predicting the climb motion of dislocation.

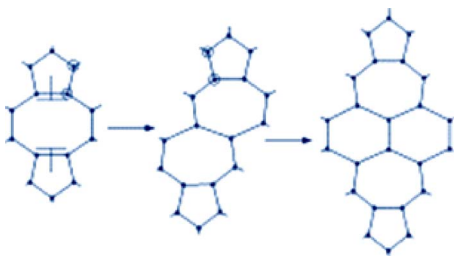

Fig. 4 Climb motion of dislocation due to sequential removal of two atom pairs (circled atoms) [29]

5 Carbon Nanotube Modeling and Simulation

As explained by Belytschko et al. [12], the fracture strength of CNTs depends primarily on the inflection point of the interatomic energy and is almost independent of the dissociation energy. Therefore, since the inflection strain occurs substantially before the strain associated with bond breaking, where the formation of other bonds is expected, the independence of fracture strength to the dissociation energy provides some confidence that the modified Morse potential can give a correct picture of nanotube fracture in cases of moderate temperatures (0–500 K). It has also been reported [32] that for carbon nanotubes, the force-strain relation is highly nonlinear at the attraction region, especially at large strains, and inflection point (peak force) occurs at 19% strain. The repulsive force increases rapidly as the bond length shortens from the equilibrium length with less nonlinearity than the attractive force.

For the modeling of the C–C bonds, the carbon nanotube is considered as a space frame structure, and the 3D elastic ANSYS BEAM4 element is used to represent the covalent bond existing between the C–C atoms in the nanotube. The nonlinear behavior of the C–C bonds is assigned to the beam elements using the stepwise procedure of fracture modeling [32].

Experimental observations have revealed that topological and vacancy defects introduced during the synthesis process are commonly present in CNTs. The large differences between the theoretical predictions and experimental measurements of the Young's modulus and the tensile strength of CNTs may be a measure of the amount of defects present. Although little is known about the types of defects that might be introduced during the synthesis process, vacancy defects are likely candidates.

The current model used has the ability to consider any type of topological and vacancy defects. The modeling of defects is performed during the creation of the finite element mesh, where the necessary modifications in the nanotube lattice are made. The authors have considered two types of initial defects.

- Type I: Initial defect comprising of 10% weakening of one bond (element).
- Type II: The removal of one atom and the three bonds related to it, i.e., creating a vacancy.

Both defects are positioned at the center of the tubes. The motivation for weakening one bond is that the nanotube is a multiatom molecule, and only few defects are known that could serve as a nucleation site for fracture except for Stone–Wales dislocation. The objective for weakening one bond by Belytschko et al. [12] is to ascertain room temperature behavior, where the velocities of the atoms are random and nonzero. As the potential energy nears the inflection point due to the applied force, some bonds will be stretched beyond the point of maximum force by the kinetic energy. The intent of the 10% imperfection is to model the effect of random velocities on the behavior at nonzero temperatures.

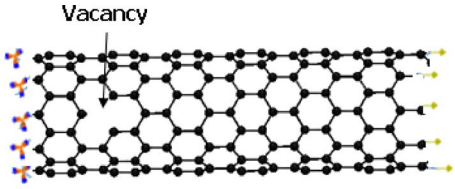

Fig. 5 Space frame model of a fixed-free carbon nanotube subjected to axial tension

In the present paper, as shown in the Fig. 5, a space frame model of a fixed-free zigzag (20,0) carbon nanotube subjected to axial incremental tensile loading is chosen. The choice of the nanotubes was made for verification purposes as both theoretical predictions and experimental measurements exist in literature.

Yu et al. [33] performed tensile experiments using arc grown multiwalled CNTs. As the multiwalled CNTs failed in a sheathlike pattern with typically only the outer nanotube failing, it was only necessary to model the outer nanotube. In that way, any interactions of the outer nanotube with the inner tubes were neglected.

The numerical results obtained from the above mentioned model are compared with both the experimental measurements of Yu et al. [33] and the MM simulations of Belytschko et al. [12].

Considering the validation of the current space frame model using the experimental [33] and theoretical results [12], the stress intensity factors and J-integrals are calculated for various combinations of the CNT model and the crack location. The modulus of elasticity, the max tensile stress, and the density of CNT for modeling are taken as 1.16 TPa, 63,000 MPa, and 1330 kg/m^3, respectively.

The simulation tests have been carried out for different combinations of length, diameter, and crack positions. Length variations take place from 6 nm to 10 nm, whereas the outer diameter of the fixed-free SWCNT varied from 0.8 nm to 1.5 nm. These combinations are simulated for crack positions (a/L) from 0.1 to 0.9. The initial crack orientation is taken along the periphery. During the numerical solution for the stress intensity factor and the

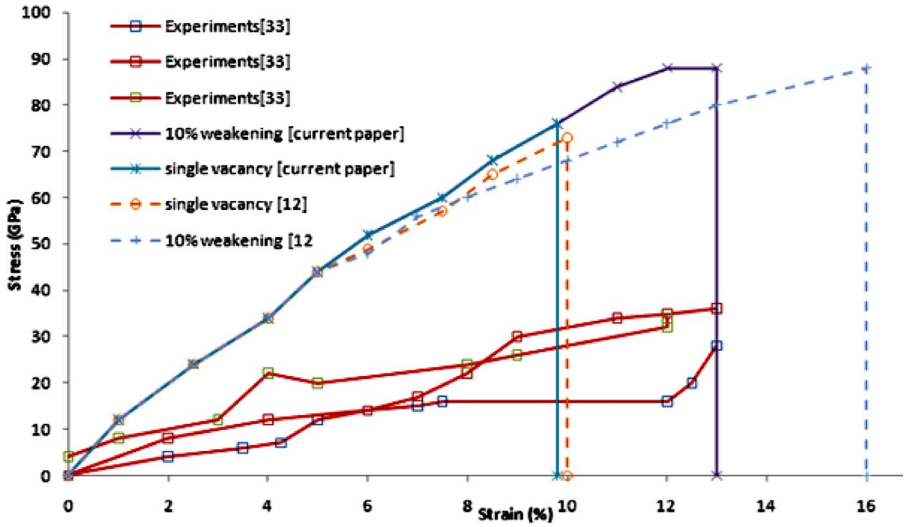

Fig. 6 Comparison of stress-strain curves predicted for the (20,0) tube with the corresponding theoretical [12] and experimental [33] curves from literature

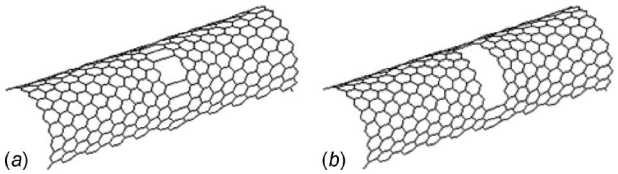

Fig. 7 Half CNT crack model with $a/L=0.5$ indicating crack propagation in atomic structure [12]

J-integral for above combinations, the half crack length to diameter ratio is kept constant. CNT is subjected to a tensile loading.

6 Results

6.1 Stress-Strain Curve. Figure 6 showed the comparison of stress-strain curves predicted by the current model for the (20,0) tube with those obtained by the MM simulations of Chandra et al. [11] and the experiments of Yu et al. [33].

Yu et al. [33] performed several experiments whose stress-strain curves showed very large dispersion. As the comparison with the whole number of the curves would be valueless, three of those, which show the best correlation, have been included in the above figure. Curves that concern both types of initial defects are displayed.

It is observed that the model used here significantly overestimates the Young's modulus and strength of CNTs. The most possible cause for this discrepancy was the defects of unknown type and amount that appeared in the nanotubes tested by Yu et al. [33]. Mielke et al. [13] found that approximately large circular holes, which would be consistent with damage resulting from harsh oxidative purification processes, may substantially reduce the failure stresses and failure strains of CNTs, providing a likely explanation for the discrepancy. Specifically, Mielke et al. [13] found that the one- and two-atom vacancy defects reduced the failure stresses by as much as 26%, thus approaching the experimental failure stresses. Another possible cause, as stated by Belytschko et al. [12], is the slippage that possibly occurred at the attachments for the high strain cases reported in Yu et al. [33], resulting in a decrease in the measured values of nanotube Young's modulus.

A very good agreement is achieved for the results obtained by the current model and the MM simulations [12]. The curves obtained by the two methods for both types of initial defects coincide up to 6% strain, giving the same Young's modulus for the

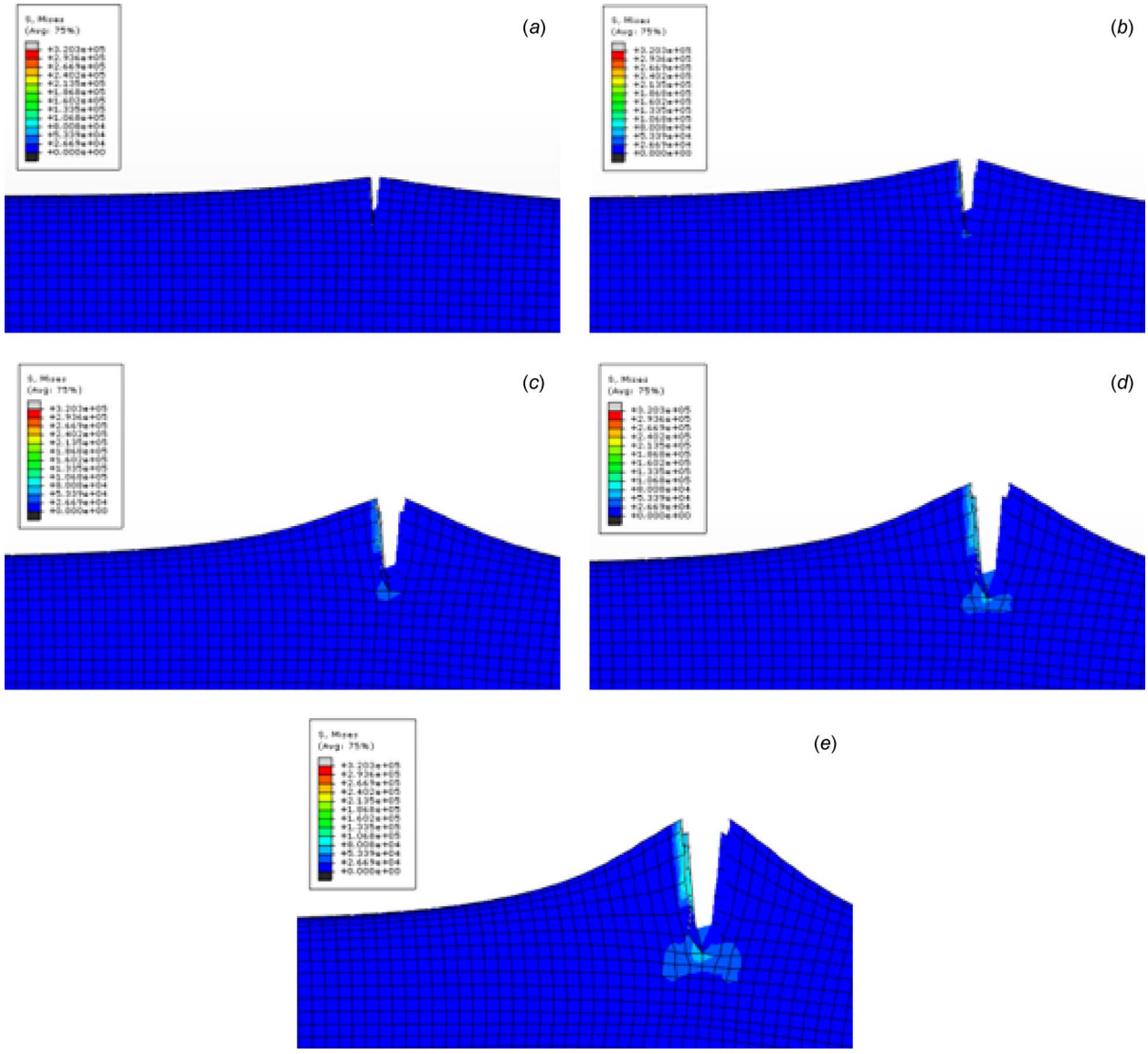

Fig. 8 ((*a*)–(*e*)) Progressive fracture models of SWCNT using XFEM

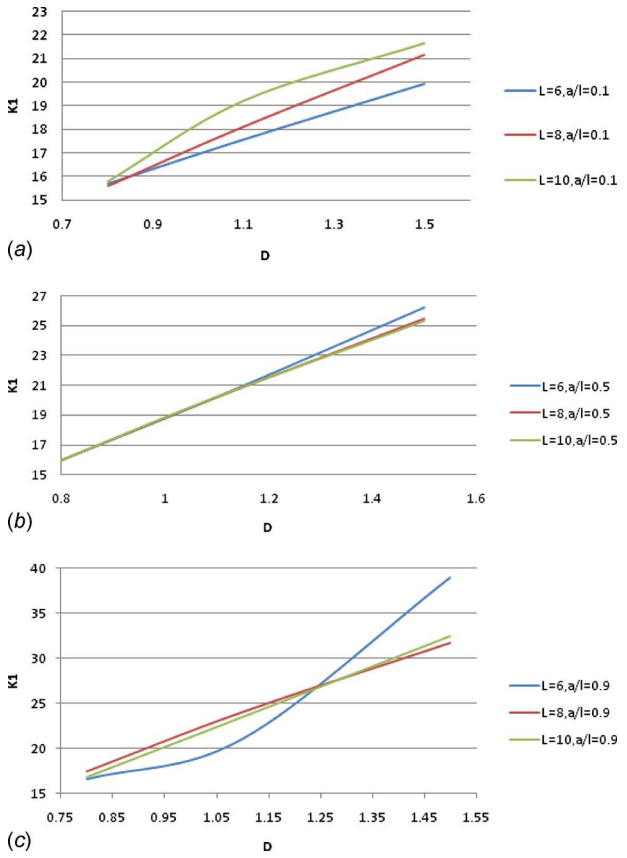

Fig. 9 Variations in stress intensity factor with the changes in length and diameter for (*a*) $a/L=0.1$, (*b*) $a/L=0.5$, and (*c*) $a/L=0.9$

nanotubes. For strains larger than 6%, the current model predicts higher Young's modulus than MM simulations. This difference is much smaller in the case of type II defect since the analyses of both models stop at around 9.5–10% strain. Regarding failure strain, in the case of type II defect, the fracture strain predicted by the current model agrees very well with the one reported by Belytschko et al. [12], while in the case of the type I defect, it shows a considerable difference (13.12% against 16%). Nevertheless, the fracture strain predicted by the model in this case (13.12%) was equal to the one obtained by two different experiments of Yu et al. [33]. These results show that the current model explained above can be used for further investigation using XFEM.

6.2 Crack Propagation Using XFEM. Crack propagation in the solid model of CNT is done using XFEM for the current space frame model. Crack in SWCNT is orientated in the lateral direction. The half crack length to diameter ratio (c/D) is 0.02. Figure 7 shows a half CNT crack model with the crack position at $a/L=0.5$ in atomic structure. Level set method is used for the crack propagation in CNT.

Figure 8 shows progressive crack propagation in the solid model of CNT for $a/L=0.5$, length=6 nm, and diameter =1.2 nm. As crack progresses, stresses at the crack tip is found to increase, and the value of the von Mises stress goes up to 3.2 $\times 10^5$ pN/nm^2. Stress intensity factors and J-integrals are calculated and specific patterns are found for various combinations of the CNT model and the crack location. As the load condition considered here is purely tensile, the stress intensity factor K_1 plays a more significant role, whereas stress intensity factors K_2 and K_3 are found nearly equal to zero and, hence, can be ignored.

Figure 9 shows the variation of the stress intensity factor K_1 with the crack location for various length combinations. Results

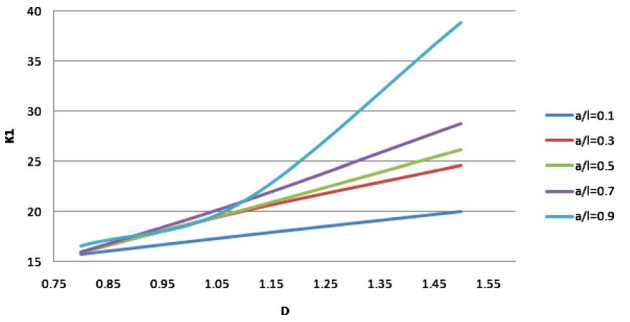

Fig. 10 SIF for different crack positions along the length of SWCNT

show the effect of change in the stress intensity factor with the change in the length and the diameter. It is observed that the change in diameter has a greater impact on the stress intensity factor as compared with the length. Also, for the same diameter and different length conditions, K_1 is dependent on location.

Figure 9(*a*) shows the variation of K_1 for $a/L=0.1$. It is observed that for the smaller length of nanotube, as the diameter increased, the stress intensity factor is linearly varied while for the longer nanotube, the variation in stress intensity factor is nonlinear. Thus, it is very difficult to characterize the influence of load or deformation on the magnitude of the crack-tip stress and strain fields for longer carbon nanotubes. It is clear that the increase in length leads to an increase in the stress intensity factor.

Figure 9(*b*) indicates that when the crack is at the center ($a/L=0.5$), the variation with length is nearly negligible. It can be observed from Fig. 9(*c*) that as the crack is oriented closer to the loading end ($a/L=0.9$), the stress intensity factor shows higher sensitivity to smaller lengths, which indicates more chances for crack propagation and CNT breakage. The variation of the SIF is found to be of nonlinear nature with the normal operating point corresponding to a diameter of around 1.2 nm.

Figure 10 shows a more clear view of the effect of diameter change for various values of a/L. The graph shows that if the crack is at the loading end, then the change in the value of K_1 with diameter is exponential, whereas it shows constant increase for all other locations. The J-integral also shows the same pattern as K_1.

7 Conclusions

A summary of the main conclusions of this research are as follows.

1. An atomistic-based model able to simulate the mechanical performance of CNTs by taking into account initial topological and vacancy defects is proposed. The model treats CNTs as space frame structures.
2. The numerical results obtained are compared with MM simulations and experimental measurements from literature. The results agree very well with the corresponding results of the MM simulations in all cases examined, contrary to failure strain, which shows a small discrepancy.
3. Regarding the comparison with the experimental measurements, the model overestimates stiffness and strength of the nanotubes. This discrepancy is also obtained by other theoretical models and is possibly due to the neglecting of defects of unknown type and amount that are present in the nanotubes tested.
4. This justification is supported by the findings of the current work and other theoretical works that indicate that vacancy defects, which are consistent with damage resulting from harsh oxidative purification processes, significantly reduce the strength of nanotubes. It was found that the presence of type II initial vacancy defect reduces the tensile strength of the (20,0) tube with regard to type I defect by about 17%.

5. XFEM is used for crack (fracture) propagation in CNT and contour integral technique is used to calculate stress intensity factors and J-integrals.
6. Crack propagation results show that the crack tends to propagate in the same direction as the initial one. During the entire analysis, the half crack length to diameter ratio (c/D) is kept constant.
7. For the same length and diameter, the crack located toward the higher loading end is the SIF and the J-integral. So, if the CNT is having a crack near the loading end, the severity is more, and there are more chances for crack propagation and CNT breakage. The change in the diameter of CNT affects the SIF as well as the J-integral.

References

[1] Ratner, M., and Ratner, D., 2003, *Nanotechnology: A Gentle Introduction to the Next Big Idea*, Prentice-Hall, Englewood Cliffs, NJ.

[2] Goddard, W. A., III, Brenner, D. W., Lyshevski, S. E., and Iafrate, G. J., 2003, *Handbook of Nanoscience, Engineering, and Technology*, CRC, New York.

[3] Ajayan, P. M., Schadler, L. S., and Braun, P. V., 2003, *Nanocomposite Science and Technology*, Wiley-VCH, Weinheim.

[4] Dunlap, B. I., 1994, "Relating Carbon Tubules," Phys. Rev. B, **49**, pp. 5643–5651.

[5] Joshi, A. Y., Bhatnagar, A., Harsha, S. P., and Sharma, S. C., 2010, "Vibration Response Analysis of Doubly Clamped Single Walled Wavy Carbon Nanotube Based Nano Mechanical Sensors," ASME J. Nanotechnol. Eng. Med., **1**(3), p. 031004.

[6] Joshi, A. Y., Harsha, S. P., and Sharma, S. C., 2010, "The Effect of Pinhole Defect on Dynamic Characteristics of Single Walled Carbon Nanotube Based Mass Sensor," J. Comput. Theor. Nanosci., unpublished.

[7] Joshi, A. Y., Sharma, S. C., and Harsha, S. P., 2010, "Dynamic Behaviour of Chiral Fixed-Free Single Walled Carbon Nanotube Based Nano Mechanical Sensors Due to Atomic Vacancies," Proc. Inst. Mech. Eng., Part N: Nanoeng. Nanosyst., unpublished.

[8] Joshi, A. Y., Harsha, S. P., and Sharma, S. C., 2010, "Vibration Signature Analysis of Single Walled Carbon Nanotube Based Nano Mechanical Sensors," Physica E (Amsterdam), **42**(8), pp. 2115–2123.

[9] Joshi, A. Y., Sharma, S. C., and Harsha, S. P., 2010, "Dynamic Analysis of a Clamped Wavy Single Walled Carbon Nanotube Based Nano Mechanical Sensors," ASME J. Nanotechnol. Eng. Med., **1**(3), p. 031007.

[10] Ebbesen, T. W., and Takada, T., 1995, "Topological and sp^3 Defect Structures in Nanotubes," Carbon, **33**(7), pp. 973–978.

[11] Chandra, N., Namilae, S., and Shet, C., 2004, "Local Elastic Properties of Carbon Nanotubes in the Presence of Stone–Wales Defects," Phys. Rev. B, **69**, p. 094101.

[12] Belytschko, T., Xiao, S. P., Schatz, G. C., and Ruoff, R. S., 2002, "Atomistic Simulations of Nanotube Fracture," Phys. Rev. B, **65**, p. 235430.

[13] Mielke, S. L., Troya, D., Zhang, S., Li, J.-L., Xiao, S., Car, R., Ruoff, R. S., Schatz, G. C., and Belytschko, T., 2004, "The Role of Vacancy Defects and Holes in the Fracture of Carbon Nanotubes," Chem. Phys. Lett., **390**, pp. 413–420.

[14] Liew, K. M., He, X. Q., and Wong, C. H., 2004, "On the Study of Elastic and Plastic Properties of Multi-Walled Carbon Nanotubes Under Axial Tension Using Molecular Dynamics Simulations," Acta Mater., **52**, pp. 2521–2527.

[15] Mohammadi, S., 2008, *Extended Finite Element Method for Fracture Analysis of Structures*, Blackwell, Malden, MA.

[16] Shih, C. F., and Asaro, R. J., 1988, "Elastic-Plastic Analysis of Cracks on Bimaterial Interfaces: Part I—Small Scale Yielding," ASME J. Appl. Mech., **55**, pp. 299–316.

[17] Barnett, D. M., and Asaro, R. J., 1972, "The Fracture Mechanics of Slit-Like Cracks in Anisotropic Elastic Media," J. Mech. Phys. Solids, **20**, pp. 353–366.

[18] Duarte, C., and Oden, J., 1995, "HP Clouds a Mesh Less Method to Solve Boundary-Value Problems," TICAM, Technical Report No. 95-05.

[19] Melenk, J. M., and Babuska, I., 1996, "The Partition of Unity Finite Element Method: Basic Theory and Applications," Comput. Methods Appl. Mech. Eng., **139**(1-4), pp. 289–314.

[20] Dolbow, J., 1999, "An Extended Finite Element Method With Discontinuous Enrichment for Applied Mechanics," Ph.D. thesis, Northwestern University, Evanston, IL.

[21] Dolbow, J., Moes, N., and Belytschko, T., 2000, "Discontinuous Enrichment Infinite Elements With a Partition of Unity Method," Finite Elem. Anal. Design, **36**, pp. 235–260.

[22] Moës, N., Dolbow, J., and Belytschko, T., 1999, "A Finite Element Method for Crack Growth Without Remeshing," Int. J. Numer. Methods Eng., **46**, pp. 131–150.

[23] Sukumar, N., Moes, N., Moran, B., and Belytschko, T., 2000, "Extended Finite Element Method for Three-Dimensional Crack Modeling," Int. J. Numer. Methods Eng., **48**(1549–1570), pp. 289–314.

[24] Strouboulis, T., Babuska, I., and Copps, K., 2000, "The Design and Analysis of the Generalized Finite Element Method," Comput. Methods Appl. Mech. Eng., **181**, pp. 43–69.

[25] Strouboulis, T., Babuska, I., and Copps, K., 2001, "The Generalized Finite Element Method," Comput. Methods Appl. Mech. Eng., **190**, pp. 4081–4193.

[26] Strouboulis, T., Babuska, I., and Copps, K., 2000, "The Generalised Finite Element Method: An Example of Its Implementation and Illustration of Its Performance," Int. J. Numer. Methods Eng., **47**, pp. 1401–1417.

[27] Duarte, C., Babuska, I., and Oden, J., 2000, "Generalized Finite Element Methods for Three Dimensional Structural Mechanics Problems," Comput. Struct., **77**, pp. 215–232.

[28] Osher, S., and Sethian, J., 1988, "Fronts Propagating With Curvature Dependent Speed: Algorithms Based on Hamilton–Jacobi Formulations," J. Comput. Phys., **79**, pp. 12–49.

[29] Oswald, J., Gracie, R., Khare, R., and Belytschko, T., 2009, "An Extended Finite Element Method for Dislocations in Complex Geometries: Thin Films and Nanotubes," Comput. Methods Appl. Mech. Eng., **198**, pp. 1872–1886.

[30] Ding, F., Jiao, K., Wu, M. Q., and Yakobson, B. I., 2007, "Pseudoclimb and Dislocation Dynamics in Superplastic Nanotubes," Phys. Rev. Lett., **98**(7), p. 075503

[31] Huang, J. Y., Chen, S., Wang, Z. Q., Kempa, K., Wang, Y. M., Jo, S. H., Chen, G., Dresselhaus, M. S., and Ren, Z. F., 2006, "Superplastic Carbon Nanotubes—Conditions Have Been Discovered That Allow Extensive Deformation of Rigid Single-Walled Nanotubes," Nature (London), **439**(7074), pp. 281–282.

[32] Tserpes, K. I., Papanikos, P., and Tsirkas, S. A., 2006, "A Progressive Fracture Model for Carbon Nanotubes," Composites, Part B, **37**, pp. 662–669.

[33] Yu, M.-F., Lourie, O., Dyer, M. J., Moloni, K., Kelly, T. F., and Ruoff, R. S., 2000, "Strength and Breaking Mechanism of Multiwalled Carbon Nanotubes Under Tensile Load," Science, **287**, pp. 637–640.